Trends in Renewable Energy
OPEN ACCESS ISSN: 2376-2144
Peer-Reviewed Article futureenergysp.com/index.php/tre

Statistical Channel Modeling of Overhead Low Voltage Broadband over Power Lines (OV LV BPL) Networks – Part 2: The Numerical Results of Class Map Footprints of Real OV LV BPL Topologies, Branch Line Faults and Hook Style Energy Thefts

Athanasios G. Lazaropoulos*

School of Electrical and Computer Engineering / National Technical University of Athens / 9 Iroon Polytechniou Street / Zografou, GR 15780

Received January 22, 2020; Accepted February 26, 2020; Published March 12, 2020

In [1], the theoretical framework for the interoperability of DHM, iSHM, mSHM, the definition procedure and the class maps has been first presented for OV LV BPL networks. But the main interest of the first paper has focused on the theory of the OV LV BPL topology footprints of TIM, FIIM and HS-DET method on the class maps.
In this paper, the numerical results concerning the application of iSHM, mSHM, the definition procedure and the class maps to OV LV BPL networks are first shown. Then, given the iSHM and mSHM class maps, the footprints of TIM, FIIM and HS-DET method databases for the OV LV BPL topologies are highlighted. Finally, a technique for the detection of branch line faults and hook style energy thefts that is based on iSHM and mSHM footprints is proposed.

Keywords: Smart Grid; Broadband over Power Lines (BPL) networks; Power Line Communications (PLC); Distribution and Transmission Power Grids; Capacity; Statistics; Modeling

**Corresponding author:* AGLazaropoulos@gmail.com

Tr Ren Energy, 2020, Vol.6, No.1, 88-109. doi: 10.17737/tre.2020.6.1.00113

Nomenclature

AAAC	All Aluminum Alloy Conductor
AWGN	Additive White Gaussian Noise
BPL	Broadband over Power Lines
BPMN	Business Process Model and Notation
CASD	Channel Attenuation Statistical Distribution
CDF	cumulative density function
CS2 module	Coupling Scheme version 2 module
DHM	deterministic hybrid model
EMI	ElectroMagnetic Interference
FIIM	Fault and Instability Identification Methodology
FL noise model	Flat noise model
HS-DET method	hook style energy theft detection method
HV	High Voltage
ICT	Information and Communication Technology
IPSD limits	injected power spectral density limits
IP	Internet Protocol
iSHM	initial Statistical Hybrid Model
LOS	Line-of-Sight
LV	Low Voltage
L1PMA	L1 Piecewise Monotonic Approximation
MLE	Maximum Likelihood Estimator
mSHM	modified Statistical Hybrid Model
MTL	multiconductor transmission line
MtM	MultiWire-to-MultiWire
MV	Medium Voltage
OV	Overhead
PES	Percent Error Sum
PSD	Power spectral density
SG	Smart Grid
SHM	Statistical Hybrid Model
TIM	Topology Identification Methodology
TL	Transmission Line
TM2 method	Transmission Matrix version 2 method
UN	Underground
WtG	Wire-to-Ground
WtW	Wire-to-Wire

1. Introduction

In SG applications, ICT is their key aspect while among the available ICT solutions, BPL technology presents some natural advantages that render the related BPL networks as the most suitable implementation for SG applications [2]. However, BPL networks operate across a hostile medium for communications since transmission and distribution power grid infrastructure and equipment have been designed to deliver power rather than information [1], [3]-[7].

The interaction results of the deterministic framework, which is represented by the DHM [3], [4], [8]-[13], and the recently proposed statistical framework, which is characterized by the SHM operation [14]-[19], for the OV LV BPL networks are presented in this paper with respect to the class maps and the footprint area concept that have been first presented for OV LV BPL networks in [1]. In detail, the numerical results of the application of iSHM and mSHM are presented while the performance of different CASDs among the available ones of iSHM and mSHM is here assessed. Actually, the most successful CASD among the available ones of iSHM is going to be identified with respect to the metrics of percentage change and the average absolute percentage change as the most successful CASD of mSHM is the Empirical one. Then, the definition procedure is going to be applied in OV LV BPL networks enriching the corresponding topology classes with topology subclasses whose respective virtual indicative OV LV BPL topologies are statistically defined in terms of the applied SHM version and its corresponding successful CASD parameters (*i.e.*, MLEs and CDF for iSHM and mSHM CASDs, respectively). On the basis of the most successful CASDs of iSHM and mSHM, the definition procedure gives as output the class maps of OV LV BPL networks that illustrate the borders between the BPL topology classes and also corresponds each CASD parameter pair to its BPL topology subclass average capacity for given power grid type, SHM version, CASD, coupling scheme, IPSD limits and noise levels [1]. By taking into account OV LV BPL topologies, the numerical results concerning the footprints on the class maps, which have been theoretically defined in [1] and may allow the impact investigation of critical events of the operation of OV LV power grids, are here presented, namely: (i) The footprint of the real OV LV BPL topologies is going to first be illustrated on the class maps thus separating the real OV LV BPL topologies from the virtual ones of class maps by exploiting the TIM database [20]; (ii) for given real indicative OV LV BPL topology, the footprint of all the corresponding OV LV BPL topologies with a sole branch line fault is going to be shown on class maps by exploiting the FIIM database [20]; and (iii) for given real indicative OV LV BPL topology, the footprint of all the corresponding OV LV BPL topologies with a single hook for energy theft are going to be demonstrated on class maps by exploiting the HS-DET method [21]. On the basis of the impact investigation of the aforementioned three critical events, the study of iSHM and mSHM footprints can also act as a useful supplementary technique for identifying branch line faults and hook style energy thefts.

The rest of this paper is organized as follows: In Section II, the numerical results concerning the interoperability of DHM, iSHM, mSHM, the definition procedure and the class maps of OV LV BPL networks are demonstrated. The footprints of the aforementioned three critical events during the operation of the OV LV BPL networks are illustrated on the class maps. Apart from the presentation, interesting comparisons

with OV MV and OV HV BPL networks are provided while the proposed technique for identifying branch line faults and hook style energy thefts through iSHM and mSHM footprints is provided.

2. Numerical Results and Discussion

In this Section, numerical results concerning the statistical behavior of OV LV BPL networks are categorized into the following subsections, namely: (i) *iSHM*: CASD MLEs of iSHM are reported while the performance of iSHM CASDs is assessed in terms of the best percentage change and average percentage change results. The best CASD of iSHM is found with respect to the aforementioned two performance metrics; (ii) *mSHM*: The performance of Empirical CASD is assessed; (iii) *Definition procedure and class maps*: The definition procedures for the best CASD of iSHM and the Empirical CASD of mSHM are applied while the corresponding class maps are illustrated; and (iv) *Footprints*: the footprints of the three OV LV BPL topology databases (*i.e.*, TIM, FIIM and HS-DET method databases) are shown on the iSHM and mSHM class maps.

2.1 CASD MLEs of iSHM for the OV LV BPL Networks

In accordance with the iSHM definition [14], [15], the BPMN diagram of iSHM, which describes its operation, is given in Fig. 2(a) of [1]. As the CASD MLEs of iSHM are concerned, these are computed at the MLE computation module of Phase C of the iSHM BPMN diagram thus affecting all the remaining iSHM operation. As already been recognized in [15], [16], the efficiency of the CASDs is based on the respective CASD MLEs that further depend on the capacity estimation of the real indicative BPL topologies that is extended to the case of OV LV BPL networks of this paper.

As the default operation settings have been assumed in [1], MLEs of the Gaussian, Lognormal, Wald, Weibull and Gumbel CASDs of iSHM are reported in Table 1 for the real indicative OV LV BPL topologies of the main subclasses of Table 1 of [1]. Similarly to [15], [16], [18], [19], the graphical analysis concerning the capacity estimation performance of CASDs of iSHM can be securely neglected by simply applying capacity estimation performance metrics such as the percentage change and the average absolute percentage change instead. Indeed, the percentage change and the average absolute percentage change of each iSHM CASD are reported in Table 2 per each indicative OV LV BPL topology main subclass as well as the capacity of each real indicative OV LV BPL topology of main subclasses.

By comparing iSHM CASD MLEs of the real indicative OV LV BPL topologies, which are presented in Table 1, with the respective ones of the real indicative OV MV BPL topologies of Table 1 of [15] and the respective ones of the real indicative OV HV BPL topologies of Table 2 of [19], iSHM CASD MLEs of the real indicative OV LV BPL topologies present more similar behavior to the iSHM CASD MLEs of the real indicative OV MV BPL topologies rather than the ones of the OV HV BPL topologies. This is due to the fact that: (i) the OV LV MTL configuration can be considered as a vertical rearrangement of the OV MV MTL configuration; and (ii) the average transmission path of OV LV BPL topologies has been assumed to be the same to the one of OV MV BPL topologies as well as the topological characteristics. Taking into account

the findings of [15], same observations concerning the iSHM CASD MLEs of the indicative OV LV BPL topologies with the ones of OV MV BPL topologies can be expressed, namely: (a) $\hat{\mu}_{MLE}^{Gaussian}$, $\hat{\mu}_{MLE}^{Lognormal}$, $\hat{\mu}_{MLE}^{Wald}$, $\hat{a}_{MLE}^{Weibull}$, $\hat{a}_{MLE}^{Gumbel}$, $\hat{\sigma}_{MLE}^{Gaussian}$, $\hat{\lambda}_{MLE}^{Wald}$

Table 1
iSHM CASD MLEs of Real Indicative OV LV BPL Topologies of Table 1 of [1] for the Default Operation Settings

Topology Name	BPL Topology Class Description	Gaussian MLEs		Lognormal MLEs		Wald MLEs		Weibull MLEs		Gumbel MLEs	
		$\hat{\mu}_{MLE}^{Gaussian}$	$\hat{\sigma}_{MLE}^{Gaussian}$	$\hat{\mu}_{MLE}^{Lognormal}$	$\hat{\sigma}_{MLE}^{Lognormal}$	$\hat{\mu}_{MLE}^{Wald}$	$\hat{\lambda}_{MLE}^{Wald}$	$\hat{a}_{MLE}^{Weibull}$	$\hat{\beta}_{MLE}^{Weibull}$	$\hat{a}_{MLE}^{Gumbel}$	$\hat{\epsilon}_{MLE}^{Gumbel}$
Urban case A	Typical OV MV BPL urban topology class	12.77	11.70	2.08	1.06	12.77	6.5	13.29	1.11	19.27	14.98
Urban case B	Aggravated OV MV BPL urban topology class	17.80	13.53	2.51	0.99	17.80	9.3	19.28	1.31	25.24	17.36
Suburban case	OV MV BPL suburban topology class	7.50	9.85	1.20	1.45	7.50	1.1	6.62	0.81	13.41	15.93
Rural case	OV MV BPL rural topology class	2.92	2.93	0.42	1.22 2.94	2.92	1.1 9.03×10^{-10}	2.80	0.92	4.48	3.10
"LOS" case	OV MV BPL "LOS" transmission class	1×10^{-11}	0	-25.33	4×10^{-15}	1×10^{-11}	2.62×10^{3}	1×10^{-11}	∞	1×10^{-11}	0

Table 2
Percentage Change between the Average Capacity of the OV LV BPL Topology Classes and the Capacity of the Indicative Topology of the Respective Classes for the Five Examined CASDs of iSHM when the Default Operation Settings are assumed
(grey background: best results, black background: unsuccessful capacity estimation)

Indicative OV LV BPL Topology Name (OV LV Capacity in Mbps)	BPL Topology Class Description	Percentage Change (%)				
		iSHM				
		Gaussian	Lognormal	Wald	Weibull	Gumbel
Urban case A (275)	Typical BPL urban class	-3.43	0.86	4.12	0.008	-6.29
Urban case B (234)	Aggravated BPL urban	-3.88	1.72	9.90	0.068	-5.58
Suburban case (322)	BPL suburban class	-4.21	-0.93	3.70	-0.11	-8.72
Rural case (361)	BPL rural class	-0.63	-0.54	0.02	-0.01	-1.17
Average Absolute Percentage Change (%)		**3.04**	**1.01**	**4.43**	**0.05**	**5.44**

and $\hat{\epsilon}_{\mathbf{MLE}}^{\mathbf{Gumbel}}$ of OV LV BPL topologies increase as the multipath environment of the OV LV BPL topologies becomes more intense; and (b) $\hat{\sigma}_{\mathbf{MLE}}^{\mathbf{Lognormal}}$ and $\hat{\beta}_{\mathbf{MLE}}^{\mathbf{Weibull}}$ of OV LV BPL topologies receive very close values among them that anyway may act as an identity value of the power grid type (*i.e.*, in this case OV LV) rather than OV LV BPL topology identifier.

In accordance with [16], [15], [18], [19], it has been proven that the capacity performance success can be assessed by applying the metrics of capacity, capacity percentage change and average absolute capacity percentage change, as reported in Table 2. More specifically:

- iSHM CASD capacity estimation performance for OV LV BPL subclasses presents similarities with the one of OV MV BPL subclasses rather than the one of OV HV BPL subclasses. Since OV distribution BPL topologies are mainly characterized by the significant lower 1km long transmission paths in comparison with the 25km long transmission paths of OV HV BPL topologies, which implies a weaker "LOS" attenuation mechanism, and by the multipath aggravation due to the frequent and relatively short branches of distribution power grids, it is evident that a CASD separation may occur on the basis of the examined power grid level.
- Similarly to OV MV BPL topology subclasses, Weibull CASD succeeds in satisfying the 3% absolute threshold of percentage change and average absolute percentage change in all the OV LV BPL topology subclasses examined. Actually, Weibull CASD achieves the best percentage change and average absolute percentage change in all the cases examined (see grey background in the column of Weibull CASD in Table 2). Note that the only CASD that can produce successful capacity estimations but with significantly worse performance in comparison with the one of Weibull CASD, especially in the cases of urban environments, is Lognormal CASD. In contrast with the Gaussian CASD that operates as the best CASD in OV HV BPL networks, Gaussian, Wald and Gumbel cannot successfully operate in OV LV BPL topologies apart from the rural case that anyway resembles to the OV HV BPL signal transmission in terms of the scarce presence of branches. Here, it should be also reminded that the best fit for UN MV BPL networks is Wald CASD as outlined in [15].

In the rest of this paper, only Weibull CASD is going to be considered as the best fit CASD among the available ones of iSHM and to be applied during the following subsections of the definition procedure, class mapping and footprints.

2.2 CASD of mSHM for the OV LV BPL Networks

The BPMN diagram of mSHM is illustrated in Fig. 2(b) of [1]. In contrast with iSHM and its supported CASD MLEs, mSHM exploits the Empirical CASD through the Empirical CDF, which acts as the CASD parameter, of the coupling scheme channel attenuation difference for given OV LV BPL topology and coupling scheme. As already been recognized in [16], [18], [19], the efficiency of the mSHM CASD is based on the Empirical CDFs while it depends on the capacity estimation of the real indicative BPL topologies.

As the default operation settings have been assumed in [1] for the computation of the Empirical CDFs of mSHM and similarly to iSHM, the graphical analysis concerning

the capacity estimation performance of Empirical CASD of mSHM can be securely

Table 3
Percentage Change between the Average Capacity of the OV LV BPL Topology Class and the Capacity of the Indicative Topology of the Respective Class for the Empirical CASD of mSHM when the Default Operation Settings are assumed
(grey background: best results, black background: unsuccessful capacity estimation)

Indicative OV LV BPL Topology Name (OV LV Capacity in Mbps)	**BPL Topology Class Description**	**Percentage Change (%)**
		mSHM
		Empirical
Urban case A (275)	Typical BPL urban class	0.14
Urban case B (234)	Aggravated BPL urban	0.19
Suburban case (322)	BPL suburban class	0.09
Rural case (361)	BPL rural class	0.03
Average Absolute Percentage Change (%)		**0.11**

neglected while the aforementioned capacity estimation performance metrics are applied instead. Indeed, the percentage change and the average absolute percentage change of mSHM Empirical CASD are reported in Table 3 per each indicative OV LV BPL topology main subclass as well as the capacity of each real indicative OV LV BPL topology of main subclasses, which anyway coincides with the respective one of Table 2.

By comparing the results of Table 3 and 2, it is evident that Empirical CASD of mSHM presents a capacity performance success for the main OV LV BPL subclasses (grey background of the last column of Table 3) that can be considered to be comparable with the one of Weibull CASD of iSHM, which anyway demonstrates the best fit results. In all the main OV LV BPL subclasses examined, Empirical CASD succeeds in satisfying the 3% absolute threshold of percentage change and average absolute percentage change. As been mentioned in Sec.2.1, this is an expected result since capacity estimation performance for OV LV BPL subclasses presents more similarities with the one of OV MV BPL subclasses rather than the one of OV HV BPL subclasses. Therefore, apart from the Weibull CASD of iSHM, the Empirical CASD of mSHM is also going to be applied during the following subsections of the definition procedure, class mapping and footprints.

2.3 iSHM and mSHM Class Mapping for OV LV BPL Classes for the Default Operation Settings

Already been presented in [1], iSHM and mSHM definition procedures for OV LV BPL topologies are here applied for the class mapping. From Sec.2.2, Weibull CASD of iSHM and Empirical CASD of mSHM are considered to execute the most successful

capacity estimations for OV LV BPL topologies and for that reason the corresponding class maps are illustrated in this paper.

As the iSHM class map scenario is concerned, there are 5 pairs of $\hat{a}_{\mathbf{MLE}}^{\mathbf{Weibull}}$ and $\hat{\beta}_{\mathbf{MLE}}^{\mathbf{Weibull}}$ that are the Weibull CASD MLEs, for the respective real indicative OV LV BPL topologies of the main subclasses of Table 1 of [1]. The iSHM class map of OV LV BPL topologies is plotted in Fig. 1 with respect to $\hat{a}_{\mathbf{MLE}}^{\mathbf{Weibull}}$ and $\hat{\beta}_{\mathbf{MLE}}^{\mathbf{Weibull}}$ for the default operation settings of [1] when the average capacity of each OV LV BPL topology subclass is considered. Note that as the spacings of the horizontal axis, the spacings of the vertical axis and the capacity borders between the adjacent distribution BPL topology classes are concerned, their computation is in accordance with [18], [19].

As the mSHM class map scenario is concerned, in accordance with [17]-[19], the examined real indicative OV LV BPL topologies of the main subclasses are examined separately during the preparation of mSHM class maps. Among the five real indicative OV LV BPL topologies of the main subclasses of Table 1 of [1], three of them are of interest in this paper and are going to be investigated through mSHM class maps; say, OV LV BPL urban case A, suburban case and rural case. With reference to [1], the mSHM class map of OV LV BPL topologies is plotted in Fig. 2(a) with respect to the indicative OV LV BPL urban case A, horizontal shift h_shift and vertical shift v_shift for the default operation settings when the average capacity of each OV LV BPL topology subclass is assumed. In the same 2D contour plot, the capacity borders between the adjacent distribution BPL topology classes and the capacity of the reference indicative OV LV BPL urban case A are also shown. In Figs. 2(b) and 2(c), same plots with Fig. 2(a) are shown but for the case of the OV LV BPL suburban case and of the OV LV BPL rural case, respectively.

By observing Fig. 1 and Figs. 2(a)-(c) and by comparing them with the respective ones of [18] and [19], it is evident that iSHM and mSHM class maps of OV LV BPL topologies present more similarities with the respective ones of OV MV BPL topologies rather than of UN MV BPL topologies and of OV HV BPL topologies. Apart from the approximate same capacity border values between the adjacent distribution BPL topology classes, the pattern of iSHM class maps present the same class area notches when the distribution BPL topologies are examined in contrast with the rectangular class areas of UN MV BPL topologies and OV HV BPL topologies. Also, as the mSHM class maps are regarded, the extent and the capacity border continuity of the "LOS" class area –*i.e.*, yellow class area in Figs. 2(a)-(c)– remain very similar between the OV MV BPL topologies and OV LV BPL ones.

Anyway, it should be noted that common issues among all the iSHM and mSHM class maps of transmission and distribution BPL topologies stand that are: (i) the clear distinction between the adjacent BPL topology classes regardless of the type of the examined class map; and (ii) the same general pattern of mSHM class maps where a large "LOS" class area exists at the left of the mSHM class map and two separate aggravated urban case class areas lie at the top and bottom right of the mSHM class map.

On the basis of Fig. 1 and Figs. 2(a)-(c), the footprints of the three OV LV BPL topology databases (*i.e.*, TIM, FIIM and HS-DET method databases), which are going to be studied in Secs. 2.4-2.6, respectively, are graphically superimposed on the aforementioned iSHM and mSHM class maps.

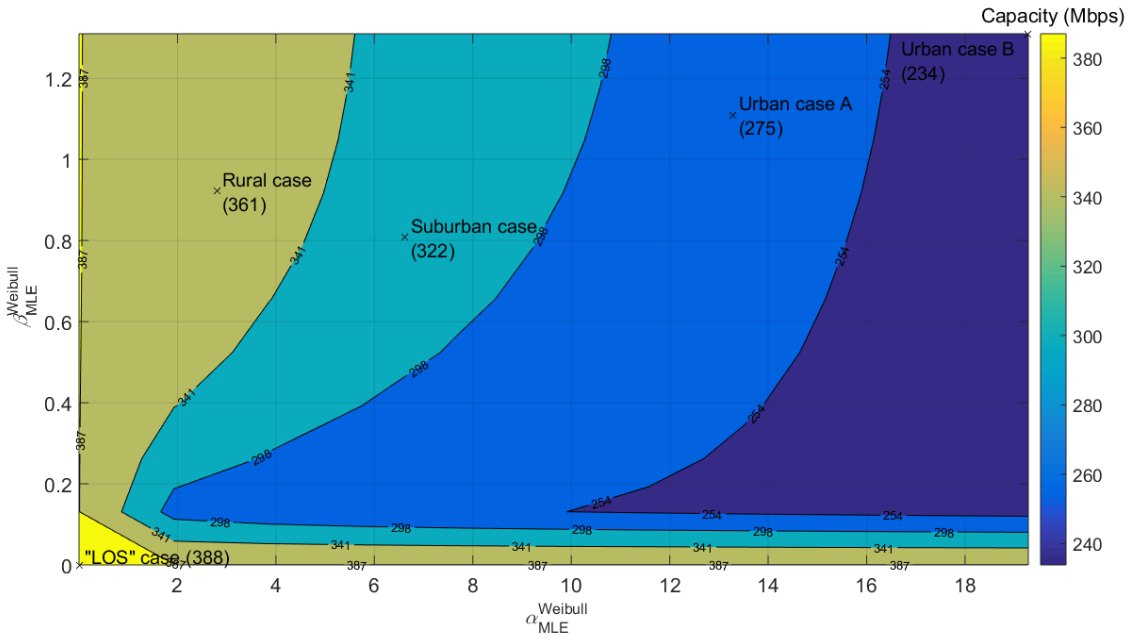

Fig. 1. iSHM class map for the average capacity of the OV LV BPL topologies in the 3-30MHz frequency band when WtG[1] coupling scheme is deployed and FCC Part 15 is applied.

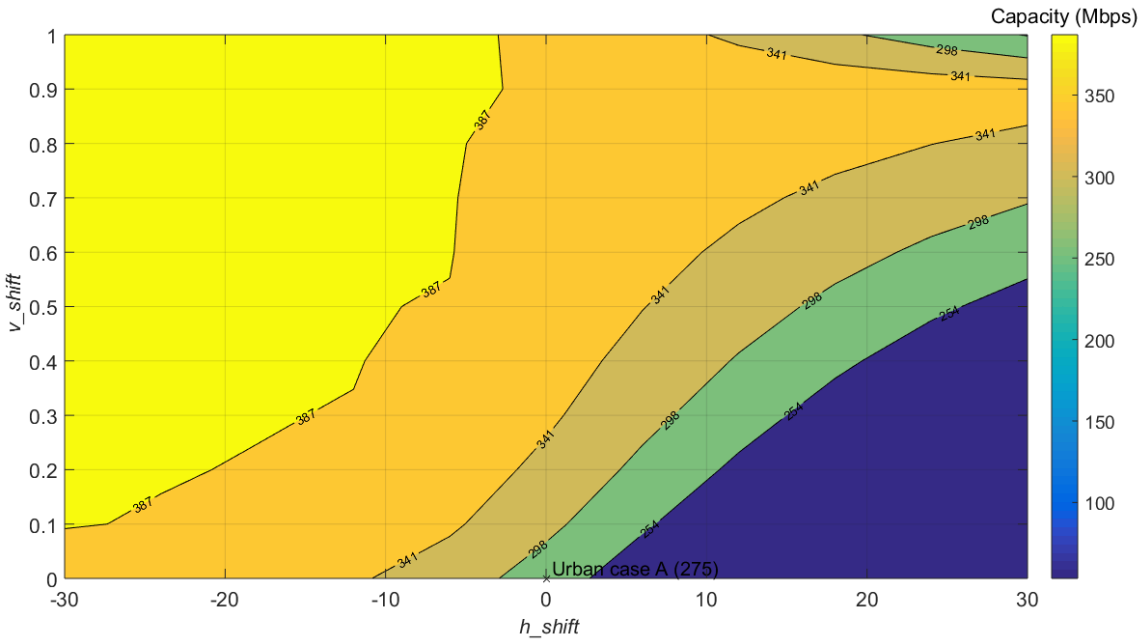
Capacity (Mbps)
v_shift
h_shift
Urban case A (275)
387
341
298
254

(a)

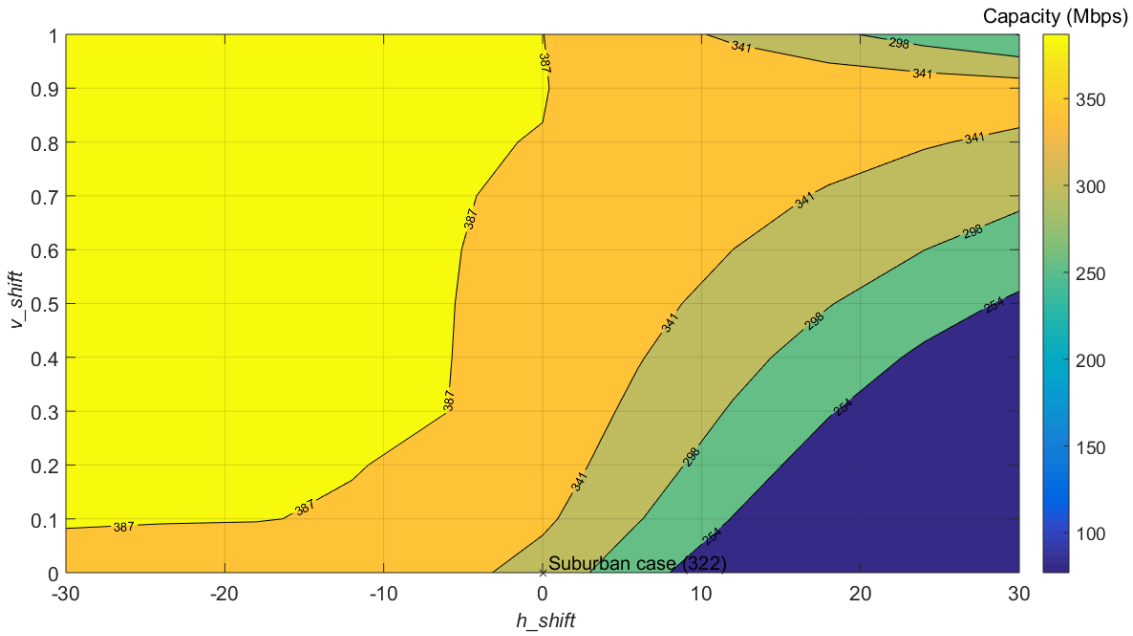
Capacity (Mbps)
v_shift
h_shift
Suburban case (322)
387
341
298
254

(b)

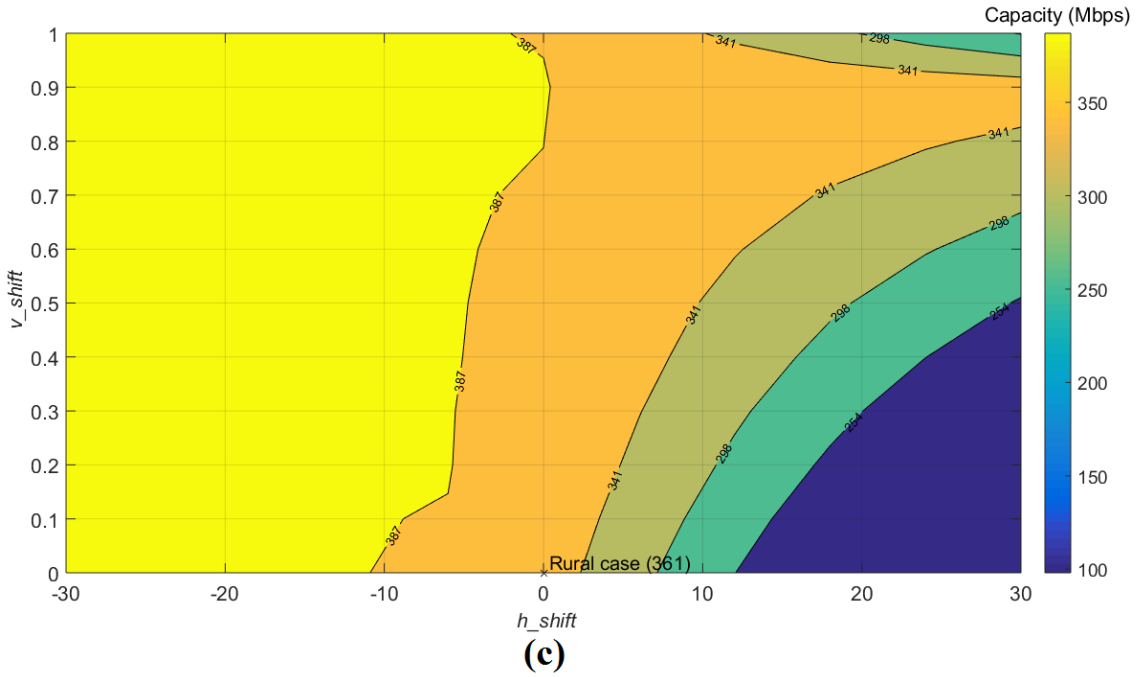

Fig. 2. mSHM class map for the average capacity of the OV LV BPL topologies in the 3-30MHz frequency band when WtG[1] coupling scheme is deployed and FCC Part 15 is applied for reference indicative OV HV BPL urban case A. (a) OV LV BPL urban case A. (b) OV LV BPL suburban case. (c) OV LV BPL rural case.

2.4 TIM Database Footprint on iSHM and mSHM Class Maps for the Default Operation Settings

In this Section, the footprint of the real OV LV BPL topologies is first illustrated on the iSHM and mSHM class maps of Sec.2.3 thus distinguishing the real OV LV BPL topologies from the virtual ones. With reference to the TIM database [20], real OV LV BPL topologies with their respective theoretical coupling scheme channel transfer functions can be retrieved. However, there is a trade-off during the preparation of the TIM database of interest between the detail degree of the assumed topological characteristics and the execution time of the theoretical coupling scheme channel transfer function and capacity computations through DHM. The TIM BPL topology database specifications that have been reported in [20] for the database preparation and affect the total execution time are the maximum number of branches N, the length spacing L_s for both branch distance and branch length and the maximum branch length L_b while typical lengths of 1000m are assumed for the real OV LV BPL topologies. To maintain realistic total execution times of the footprint representations, two different cases concerning the footprint of real OV LV BPL topologies are here examined; say, the footprints of real OV LV BPL topologies with one and two branches on iSHM and mSHM class maps. Note that the TIM BPL topology database specifications and total execution time that correspond to each scenario and class map type are also reported.

As the iSHM footprint of the real OV LV BPL topologies with one branch are concerned, the maximum number of branches N, the length spacing L_s for both branch distance and branch length and the maximum branch length L_b are assumed to be equal to

1 m, 10 m and 1000 m, respectively. With reference to the iSHM class map of Fig. 1, the iSHM footprint of the real OV LV BPL topologies with one branch is illustrated as superimposed white areas on class maps in Fig. 3(a). Similarly, the iSHM footprint of the real OV LV BPL topologies with two branches is illustrated in Fig. 3(b) when the maximum number of branches N, the length spacing L_s for both branch distance and branch length and the maximum branch length L_b are assumed to be equal to 2, 100m and 1000m, respectively.

As the mSHM footprint of the real OV LV BPL topologies with one branch are regarded, the TIM BPL topology database specifications are assumed to be the same with the ones of the iSHM footprint case. With reference to the mSHM class map of Fig. 2(c), the mSHM footprint of the real OV LV BPL topologies with one branch is illustrated as white areas in Fig. 4(a). Similarly, the mSHM footprint of the real OV LV BPL topologies with two branches is illustrated in Fig. 4(b) when the TIM BPL topology database specifications are assumed to be the same with the ones of the mSHM footprint case.

From Figs. 3(a), 3(b), 4(a) and 4(b), interesting observations concerning the iSHM and mSHM footprint planning of the real OV LV BPL topologies can be pointed out. More specifically:

- Since iSHM and mSHM class maps have already been prepared in Sec. 2.3, the total execution time considers the time that is required for the preparation of the TIM database given the TIM database specifications per each case as well as the required statistical and capacity processing. In terms of time, for the preparation of the footprints shown in Figs. 3(a), 3(b), 4(a) and 4(b), the total execution time is equal to 9674s, 7291s, 11646s, and 8567s, respectively. The different TIM database specifications regarding the two cases have been made so that the total execution time can remain relatively low without affecting the generality of the analysis. Anyway, different number of OV LV BPL topologies was expected for the two cases.
- With reference to Fig. 3(a), the iSHM footprint of OV LV BPL topologies with one branch is clearly confined in the rural case area. More specifically, as the length of the sole branch of the examined OV LV BPL topology decreases, this forces the presence of deep notches in the corresponding theoretical coupling scheme channel transfer function thus creating a richer multipath environment [12]. Conversely, the consideration of longer branches can impose more frequent but less deep notches in the corresponding theoretical coupling scheme channel transfer functions in comparison with the shorter branches. In accordance with [1], [180], OV LV BPL topologies of rare but less deep notches are characterized by increased values of $\hat{\alpha}_{\mathrm{MLE}}^{\mathrm{Weibull}}$ and $\hat{\beta}_{\mathrm{MLE}}^{\mathrm{Weibull}}$ and lower capacities. As the relative location of the OV LV BPL topologies with one short branch is concerned in the iSHM footprint, these topologies tend to be located at the lower left regions of the iSHM footprint while the OV LV BPL topologies with longer branches tend to be located at the opposite direction. Same observations can be expressed for the case of OV LV BPL topologies with two branches, where OV LV BPL topologies of two branches remain in the suburban case area with similar branch length behavior regarding the relative location in the class map suburban case area with the case of a single branch.

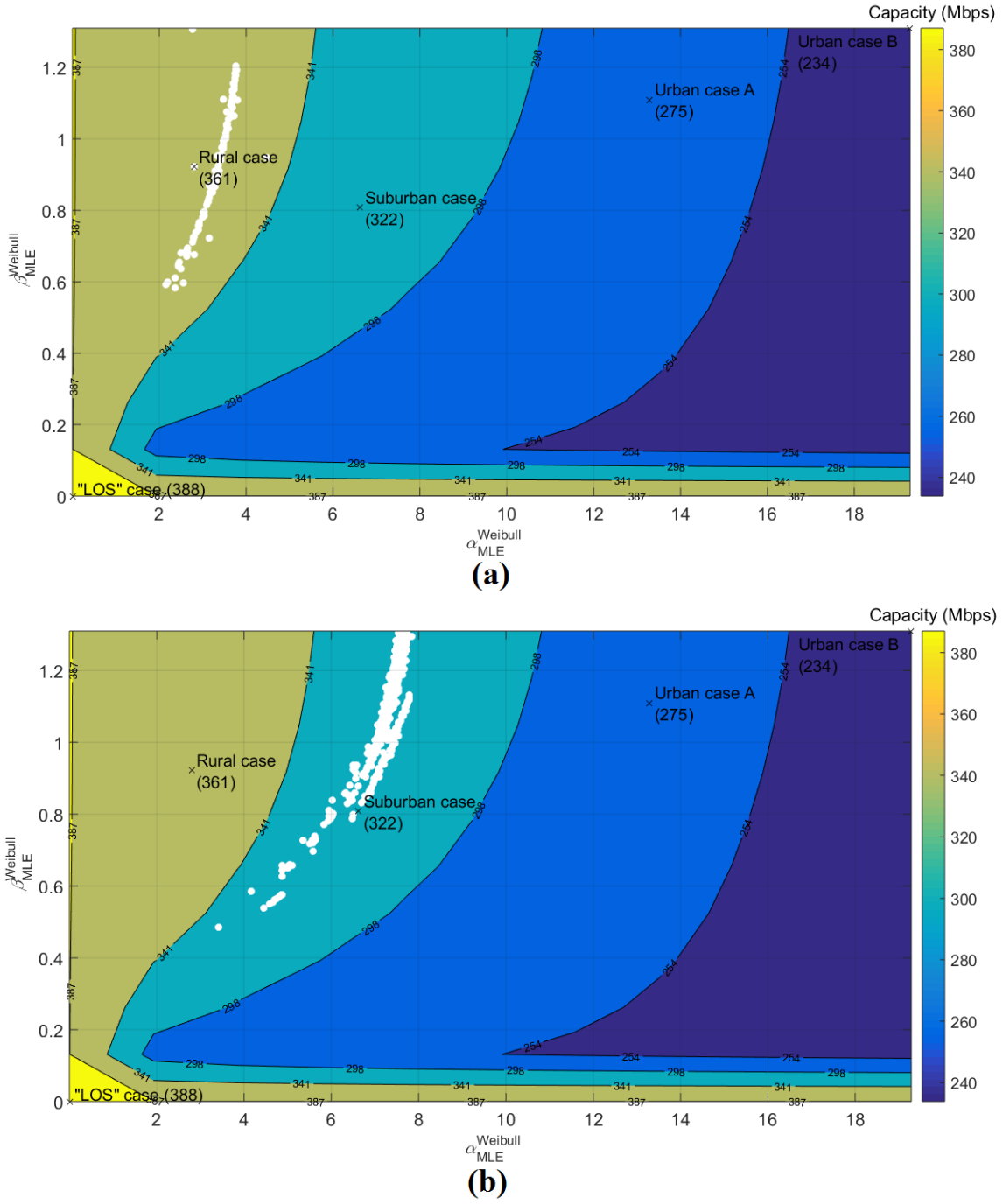

Fig. 3. Footprints of the real OV LV BPL topologies of the TIM database. (a) iSHM footprint of OV LV BPL topologies with one branch. (b) iSHM footprint of OV LV BPL topologies with two branches.

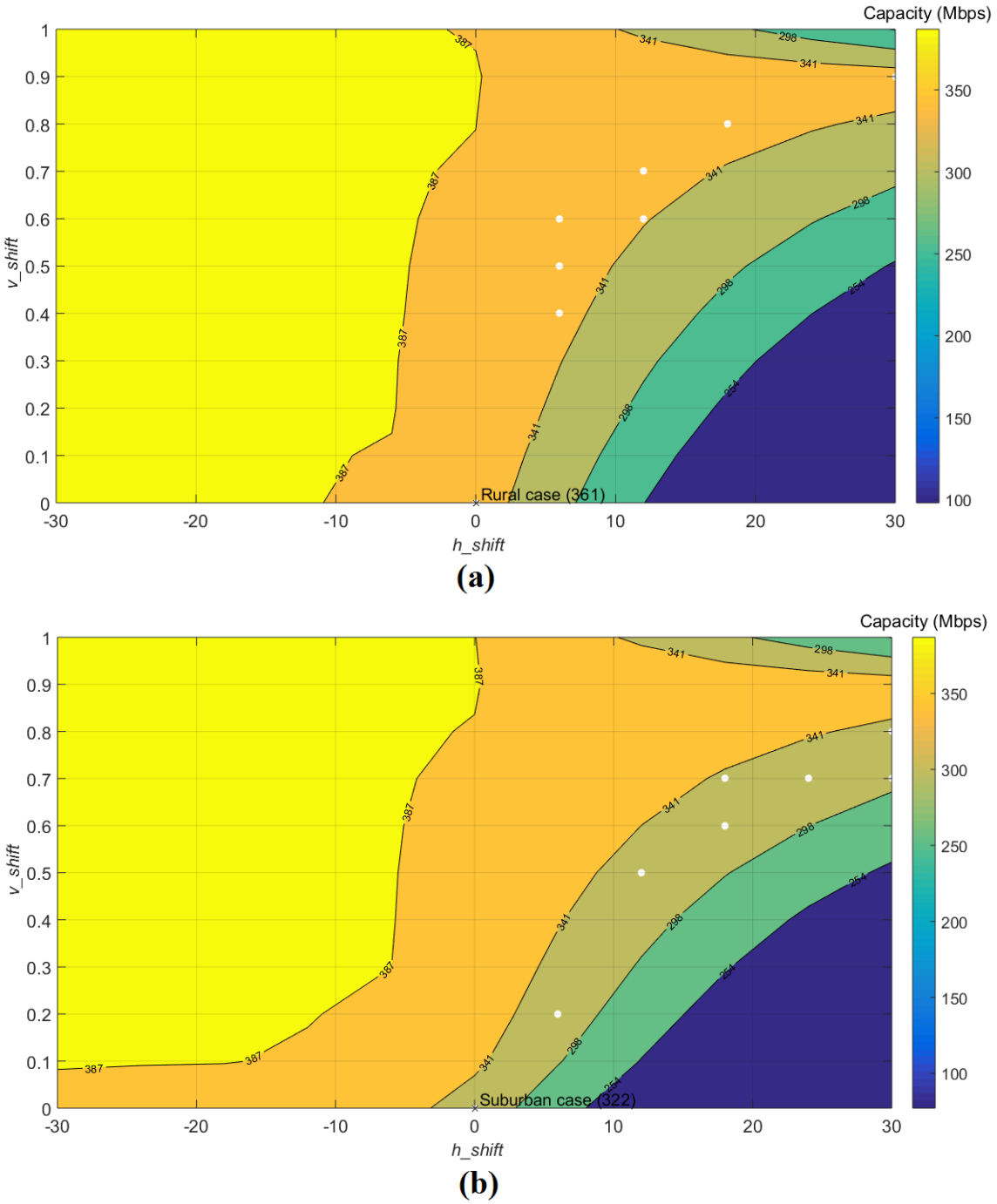

Fig. 4. Footprints of the real OV LV BPL topologies of the TIM database. (a) mSHM footprint of OV LV BPL topologies with one branch. (b) mSHM footprint of OV LV BPL topologies with two branches.

- With reference to Figs. 4(a) and 4(b), the mSHM footprints of OV LV BPL topologies with one and two branches are clearly confined in the rural and suburban case areas, respectively. Although the number of the examined OV LV BPL topologies remains the same given the number of branches, the main difference between iSHM and mSHM footprints is first their extent; this is due to

the fact that the examined real OV LV BPL topologies are characterized by their own CASD MLEs during the iSHM definition procedure and can be straightforward superimposed to iSHM class maps whereas the examined real OV LV BPL topologies are classified among the existing pairs $[h\_shift \quad v\_shift]$ of the mSHM class maps and demonstrated as white spots through the practical approximation of Frobenius distance analyzed in Sec.4.1 of [1]. As the number of spacings of the horizontal and vertical axes of the mSHM class maps of Figs. 2(a)-(c) is both equal to 10, all the white spots of Figs. 3(a) and 3(b) are classified into 8 white spots in Figs. 4(a) and 4(b), respectively. It is evident that as the number of spacings of the horizontal and vertical axes increases so does the number of white spots of the mSHM footprints of the real OV LV BPL topologies since a larger set of available pairs $[h\_shift \quad v\_shift]$ can be examined.

- The latter difference between the illustration of iSHM and mSHM footprints also explains the greater total execution times of mSHM footprints, which have been reported, in comparison with the ones of iSHM footprints for given number of branches of the real OV LV BPL topologies. As it is shown, the straightforward CASD MLE computation of iSHM definition procedure remains faster than the comparison among all the available virtual OV LV BPL topologies of each OV LV BPL topology subclass during the preparation of mSHM footprints.

2.5 FIIM Database Footprint on iSHM and mSHM Class Maps for the Default Operation Settings

In this Section, the iSHM and mSHM footprints of the real OV LV BPL topologies with a sole branch line fault are first illustrated. For given real OV LV BPL topology, say, OV LV BPL urban case A, one branch line fault is once applied to each of the three branches of the examined OV LV BPL urban case A. With reference to the FIIM database [20], real OV LV BPL topologies with one branch line fault that are based on the OV LV BPL urban case A with their respective theoretical coupling scheme channel transfer functions can be retrieved. Similarly to the TIM database specifications, appropriate FIIM BPL topology database specifications that have been reported in [1] for the database preparation are assumed, namely the fault location at each existing branch of the real indicative OV LV BPL urban case A ranges from 0.1 m to the end of the corresponding branch with a step of 0.1m. Note that the faulty branch termination is again assumed to be open-circuit.

As the iSHM footprint of the real OV LV BPL topologies with one branch line fault that are based on the real indicative OV LV BPL urban case A is concerned, the iSHM footprint of the real OV LV BPL topologies with one branch line fault is illustrated as superimposed white areas on class maps in Fig. 5 with reference to the iSHM class map of Fig. 1. Similarly to iSHM footprint of Fig. 5, the mSHM footprint of the real OV LV BPL topologies with one branch line fault that are based on the real indicative OV LV BPL urban case A is shown in Fig. 6.

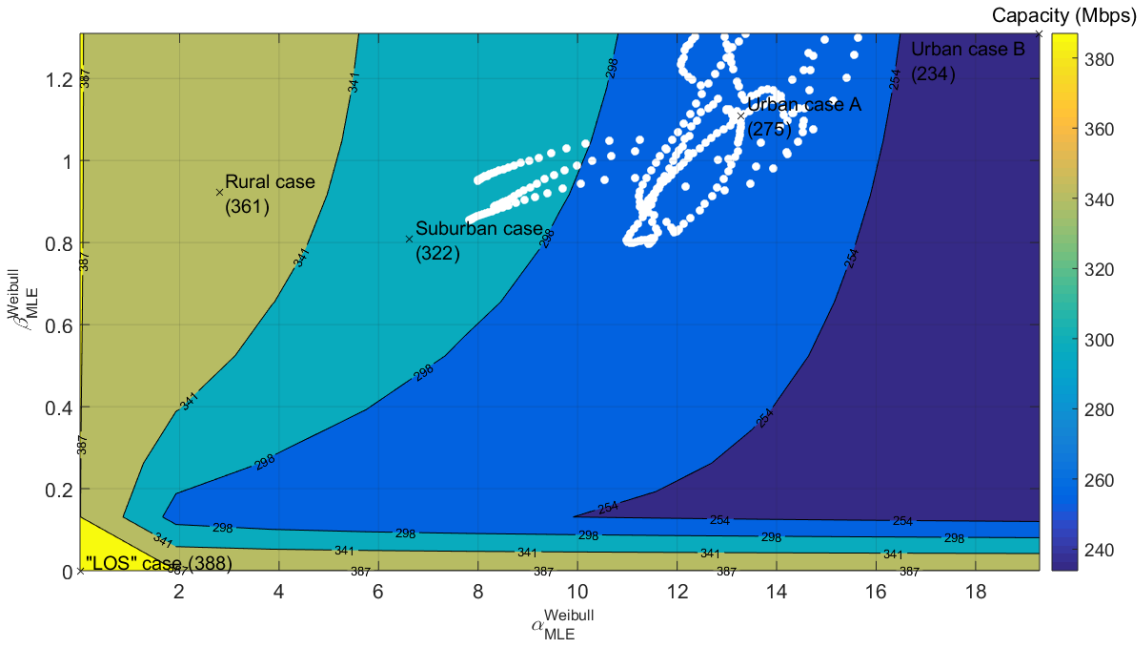

Fig. 5. iSHM footprint of the real OV LV BPL topologies of the FIIM database with one branch line fault with reference to the real indicative OV LV BPL urban case A.

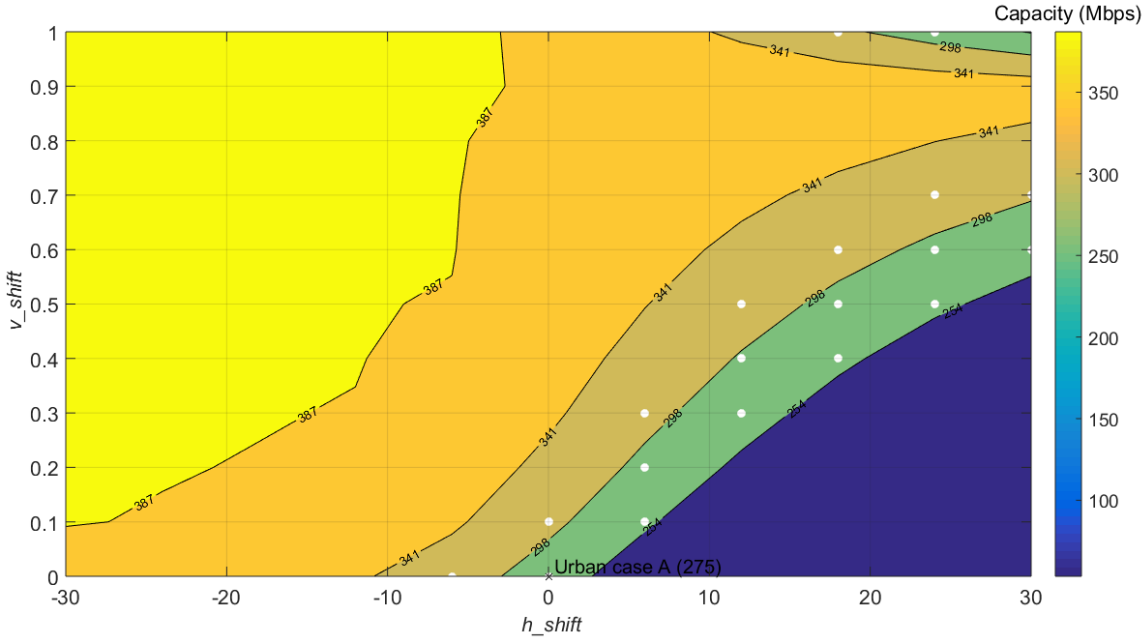

Fig. 6. mSHM footprint of the real OV LV BPL topologies of the FIIM database with one branch line fault with reference to the real indicative OV LV BPL urban case A.

From Figs. 5 and 6, it is observed that the real OV LV BPL topologies with one branch line fault, which are based on the real indicative OV LV BPL urban case A, are not strictly bounded in the class area of urban case A but are also extended to the class area of suburban case either in iSHM class map or in mSHM class map. The branch line faults of the real OV LV BPL topologies that are situated at the class area of the suburban

case are characterized by branch line lengths that are lower than approximately 2 m (short branches). This remark can be considered as the continuation of the remark of Sec.2.4, which has dealt with the relative position of OV LV BPL topologies with short branches at iSHM footprints (*i.e.*, lower left regions of the corresponding class areas). Hence, iSHM and mSHM class maps better distinguishes branch line faults of short lengths since the corresponding OV LV BPL topologies with the branch line faults violate the class area borders thus allowing their imminent detection. In general, iSHM and mSHM class maps consist of class areas that are mainly represented by real OV LV BPL topologies of different number of long branches. The last observation about iSHM and mSHM class maps introduces a new technique concerning the detection of branch line faults and energy theft hooks (see also Sec.2.6) that depends on the characterization of the examined OV LV BPL topologies in terms of their number of long branches and not on the straightforward benchmark of their spectral metrics, such as coupling scheme transfer functions and capacities presented in [21]-[28].

2.6 HS-DET Method Database Footprint on iSHM and mSHM Class Maps for the Default Operation Settings

In this Section, the iSHM and mSHM footprints of the real OV LV BPL topologies with a single hook for energy theft are first illustrated. For given real OV LV BPL topology, say, the real indicative OV LV BPL suburban case, one hook, which is treated as a new branch [21], [29], [30], is hung on the existing real indicative OV LV BPL suburban case. With reference to HS-DET method database [21], real OV LV BPL topologies with a single hook for energy theft that are based on the real indicative OV LV BPL suburban case with their respective theoretical coupling scheme channel transfer functions can be retrieved. Similarly to the TIM and FIIM database specifications, appropriate HS-DET method database specifications that have been reported in [20] for the database preparation are assumed, namely the location of the hook for energy theft that ranges from 0.1 m to 1000 m with a step of 10 m and the length of the hook that ranges from 0.1 m to 200 m with a step of 10 m. Note that the branch termination, which is used for the simulation of the hook of the energy theft, is again assumed to be open-circuit.

As the iSHM footprint of the real OV LV BPL topologies with a single hook for energy theft that are based on the real indicative OV LV BPL suburban case is concerned, the iSHM footprint of the real OV LV BPL topologies with a single energy theft hook is illustrated as superimposed white areas on class maps in Fig. 7 with reference to the iSHM class map of Fig. 1. Similarly to iSHM footprint of Fig. 7, the mSHM footprint of the real OV LV BPL topologies with a single hook for energy theft that are based on the real indicative OV LV BPL suburban case is shown in Fig. 8.

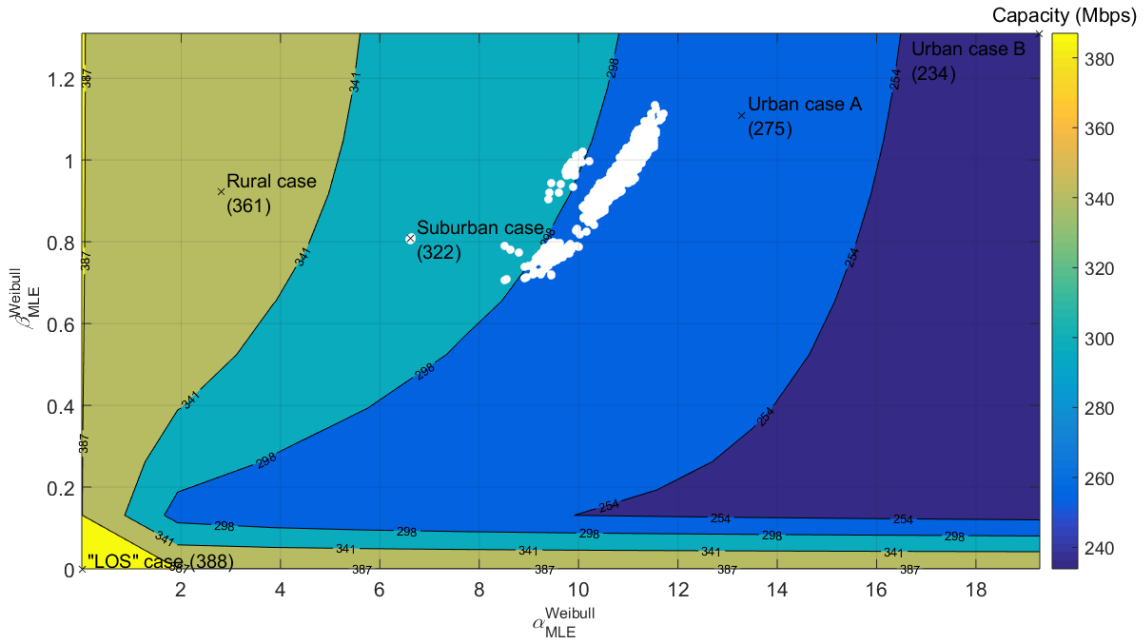

Fig. 7. iSHM footprint of the real OV LV BPL topologies of the HS-DET method database with a single hook for energy theft with reference to the real indicative OV LV BPL suburban case.

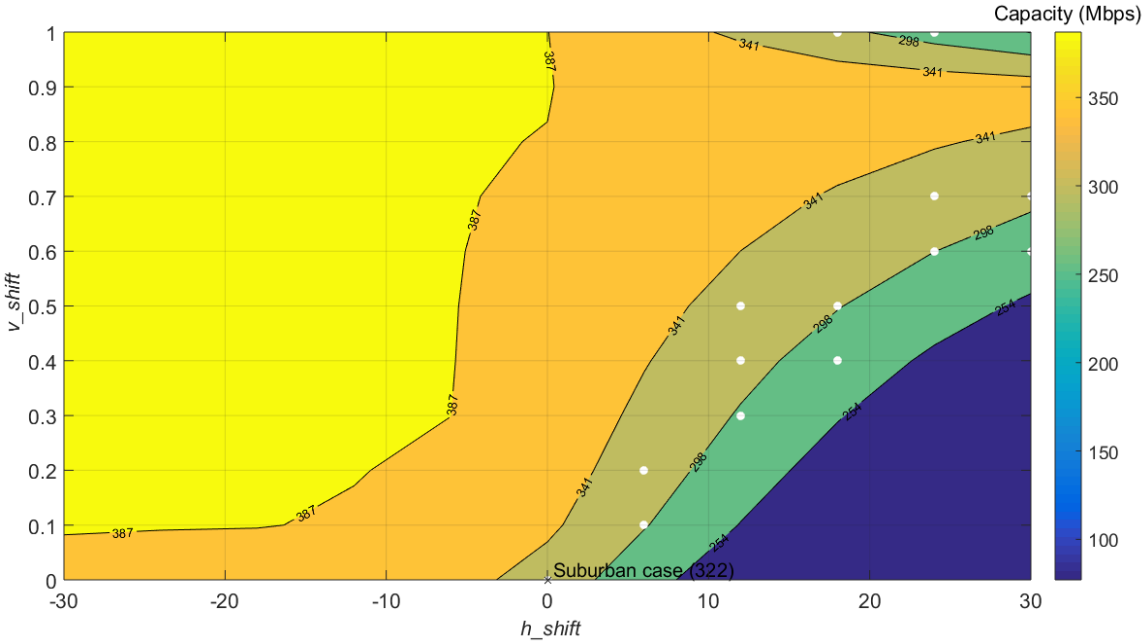

Fig. 8. mSHM footprint of the real OV LV BPL topologies of the HS-DET method database with a single hook for energy theft with reference to the real indicative OV LV BPL suburban case.

From Figs. 7 and 8, it is evident that the proposed technique concerning the detection of branch line faults through iSHM and mSHM footprints can be easily extended in order to detect hooks for energy theft. Indeed, the insertion of a single hook, which is treated by the DHM as a new branch insertion to the existing real indicative OV LV BPL suburban case, has as result the shift of the iSHM and mSHM footprints right

inside the class area of urban case A with few exceptions that remain close to the right border of the class area of suburban case; the later exceptions are real OV LV BPL topologies that derive from the real indicative OV LV BPL suburban case while short hooks for energy thefts are deployed across them. Since the relative location of iSHM and mSHM footprints is more sensitive to the number of long branches rather than the multipath environment aggravation due to the short branches, the detection of the hooks for energy theft becomes easier in comparison with the detection of the branch line faults due to the visible violation of class area borders. Here, it should be mentioned that the detection of long hooks for energy thefts that is offered by the examination of the iSHM footprints may act as supplementary technique to the HS-DET method of [21], [29]-[31] that detects more easily the short hooks for energy theft.

3. Conclusions

In this second paper, the numerical results concerning the iSHM and mSHM footprints of the OV LV BPL networks have been demonstrated as well as a new technique, which acts supplementary to the existing FIIM and HS-DET method. From iSHM and mSHM footprints of the OV LV BPL topologies it has been verified that: (i) Depending on the number of branches, the real OV LV BPL topologies are classified in the existing class areas; (ii) As the length of the branches of the real OV LV BPL topologies increases, their iSHM footprint tends to be located at the upper right regions of the corresponding class area; (iii) Branch line faults and hook style energy theft can be easily identified by studying the relative location in the corresponding class area given the real OV LV BPL topology of the basis; (iv) Hook style energy theft can be more easily detected in comparison with the branch line faults; and (v) Complimentary to FIIM and HS-DET method, which better operate with short branches, the study of iSHM and mSHM footprints can act as a useful supplementary technique for identifying branch line faults of short branches and hook style energy thefts of long hooks.

CONFLICTS OF INTEREST

The author declares that there is no conflict of interests regarding the publication of this paper.

References

[1] A. G. Lazaropoulos, “Statistical Channel Modeling of Overhead Low Voltage Broadband over Power Lines (OV LV BPL) Networks – Part 1: The Theory of Class Map Footprints of Real OV LV BPL Topologies, Branch Line Faults and Hook-Style Energy Thefts,” *Trends in Renewable Energy*, vol. 6, no. 1, pp. 61-87.

[2] G. López, J. Matanza, D. de la Vega, M. Castro, A. Arrinda, J. I. Moreno, and A. Sendin, “The Role of Power Line Communications in the Smart Grid Revisited: Applications, Challenges, and Research Initiatives,” *IEEE Access*, vol. 7, pp. 117346–117368, 2019.

[3] A. G. Lazaropoulos and P. G. Cottis, "Transmission characteristics of overhead medium voltage power line communication channels," *IEEE Trans. Power Del.*, vol. 24, no. 3, pp. 1164-1173, Jul. 2009.

[4] A. G. Lazaropoulos and P. G. Cottis, "Broadband transmission via underground medium-voltage power lines-Part I: transmission characteristics," *IEEE Trans. Power Del.*, vol. 25, no. 4, pp. 2414-2424, Oct. 2010.

[5] E. Biglieri, "Coding and modulation for a horrible channel," *IEEE Commun. Mag.*, vol. 41, no. 5, pp. 92–98, May 2003.

[6] M. Gebhardt, F. Weinmann, and K. Dostert, "Physical and regulatory constraints for communication over the power supply grid," *IEEE Commun. Mag.*, vol. 41, no. 5, pp. 84-90, May 2003.

[7] M. Götz, M. Rapp, and K. Dostert, "Power line channel characteristics and their effect on communication system design," *IEEE Commun. Mag.*, vol. 42, no. 4, pp. 78-86, Apr. 2004.

[8] A. G. Lazaropoulos, "Towards Broadband over Power Lines Systems Integration: Transmission Characteristics of Underground Low-Voltage Distribution Power Lines," *Progress in Electromagnetics Research B*, vol. 39, pp. 89-114, 2012. [Online]. Available: http://www.jpier.org/PIERB/pierb39/05.12012409.pdf

[9] A. G. Lazaropoulos and P. G. Cottis, "Capacity of overhead medium voltage power line communication channels," *IEEE Trans. Power Del.*, vol. 25, no. 2, pp. 723-733, Apr. 2010.

[10] A. G. Lazaropoulos and P. G. Cottis, "Broadband transmission via underground medium-voltage power lines-Part II: capacity," *IEEE Trans. Power Del.*, vol. 25, no. 4, pp. 2425-2434, Oct. 2010.

[11] A. G. Lazaropoulos, "Broadband transmission and statistical performance properties of overhead high-voltage transmission networks," *Hindawi Journal of Computer Networks and Commun.*, 2012, article ID 875632, 2012. [Online]. Available: http://www.hindawi.com/journals/jcnc/aip/875632/

[12] A. G. Lazaropoulos, "Towards Modal Integration of Overhead and Underground Low-Voltage and Medium-Voltage Power Line Communication Channels in the Smart Grid Landscape: Model Expansion, Broadband Signal Transmission Characteristics, and Statistical Performance Metrics (Invited Paper)," *ISRN Signal Processing*, vol. 2012, Article ID 121628, pp. 1-17, 2012. [Online]. Available: http://www.hindawi.com/isrn/sp/2012/121628/

[13] A. G. Lazaropoulos, "Broadband Performance Metrics and Regression Approximations of the New Coupling Schemes for Distribution Broadband over Power Lines (BPL) Networks," *Trends in Renewable Energy*, vol. 4, no. 1, pp. 43-73, Jan. 2018. [Online]. Available: http://futureenergysp.com/index.php/tre/article/view/59/pdf

[14] A. G. Lazaropoulos, "Statistical Broadband over Power Lines Channel Modeling – Part 1: The Theory of the Statistical Hybrid Model," *Progress in Electromagnetics Research C*, vol. 92, pp. 1-16, 2019. [Online]. Available: http://www.jpier.org/PIERC/pierc92/01.19012902.pdf

[15] A. G. Lazaropoulos, "Statistical Broadband over Power Lines (BPL) Channel Modeling – Part 2: The Numerical Results of the Statistical Hybrid Model,"

Progress in Electromagnetics Research C, vol. 92, pp. 17-30, 2019. [Online]. Available: http://www.jpier.org/PIERC/pierc92/02.19012903.pdf

[16] A. G. Lazaropoulos, "Enhancing the Statistical Hybrid Model Performance in Overhead and Underground Medium Voltage Broadband over Power Lines Channels by Adopting Empirical Channel Attenuation Statistical Distribution," *Trends in Renewable Energy*, vol. 5, no. 2, pp. 181-217, 2019. [Online]. Available: http://futureenergysp.com/index.php/tre/article/view/96/pdf

[17] A. G. Lazaropoulos, "Virtual Indicative Broadband over Power Lines Topologies for Respective Subclasses by Adjusting Channel Attenuation Statistical Distribution Parameters of Statistical Hybrid Models – Part 1: Theory," *Trends in Renewable Energy*, vol. 5, no. 3, pp. 237-257, Aug. 2019. [Online]. Available: http://futureenergysp.com/index.php/tre/article/view/99/pdf

[18] A. G. Lazaropoulos, "Virtual Indicative Broadband over Power Lines Topologies for Respective Subclasses by Adjusting Channel Attenuation Statistical Distribution Parameters of Statistical Hybrid Models – Part 2: Numerical Results for the Overhead and Underground Medium-Voltage Power Grids," *Trends in Renewable Energy*, vol. 5, no. 3, pp. 258-281, Aug. 2019. [Online]. Available: http://futureenergysp.com/index.php/tre/article/view/100/pdf

[19] A. G. Lazaropoulos, "Virtual Indicative Broadband over Power Lines Topologies for Respective Subclasses by Adjusting Channel Attenuation Statistical Distribution Parameters of Statistical Hybrid Models – Part 3: The Case of Overhead Transmission Power Grids," *Trends in Renewable Energy*, vol. 5, no. 3, pp. 282-306, Aug. 2019. [Online]. Available: http://futureenergysp.com/index.php/tre/article/view/101/pdf

[20] A. G. Lazaropoulos, "Improvement of Power Systems Stability by Applying Topology Identification Methodology (TIM) and Fault and Instability Identification Methodology (FIIM)–Study of the Overhead Medium-Voltage Broadband over Power Lines (OV MV BPL) Networks Case," *Trends in Renewable Energy*, vol. 3, no. 2, pp. 102-128, Apr. 2017. [Online]. Available: http://futureenergysp.com/index.php/tre/article/view/34

[21] A. G. Lazaropoulos, "Detection of Energy Theft in Overhead Low-Voltage Power Grids – The Hook Style Energy Theft in the Smart Grid Era," *Trends in Renewable Energy*, vol. 5, no. 1, pp. 12-46, Oct. 2018. [Online]. Available: http://futureenergysp.com/index.php/tre/article/view/81/pdf

[22] A. G. Lazaropoulos, "Measurement Differences, Faults and Instabilities in Intelligent Energy Systems – Part 2: Fault and Instability Prediction in Overhead High-Voltage Broadband over Power Lines Networks by Applying Fault and Instability Identification Methodology (FIIM)," *Trends in Renewable Energy*, vol. 2, no. 3, pp. 113-142, Oct. 2016. [Online]. Available: http://futureenergysp.com/index.php/tre/article/view/27/33

[23] A. G. Lazaropoulos, "Measurement Differences, Faults and Instabilities in Intelligent Energy Systems–Part 1: Identification of Overhead High-Voltage Broadband over Power Lines Network Topologies by Applying Topology Identification Methodology (TIM)," *Trends in Renewable Energy*, vol. 2, no. 3, pp. 85-112, Oct. 2016. [Online]. Available: http://futureenergysp.com/index.php/tre/article/view/26/32

[24] A. G. Lazaropoulos, "Power Systems Stability through Piecewise Monotonic Data Approximations – Part 1: Comparative Benchmarking of L1PMA, L2WPMA and L2CXCV in Overhead Medium-Voltage Broadband over Power Lines Networks," *Trends*

in Renewable Energy, vol. 3, no. 1, pp. 2-32, Jan. 2017. [Online]. Available: http://futureenergysp.com/index.php/tre/article/view/29/34

[25] A. G. Lazaropoulos, "Power Systems Stability through Piecewise Monotonic Data Approximations – Part 2: Adaptive Number of Monotonic Sections and Performance of L1PMA, L2WPMA and L2CXCV in Overhead Medium-Voltage Broadband over Power Lines Networks," *Trends in Renewable Energy*, vol. 3, no. 1, pp. 33-60, Jan. 2017. [Online]. Available: http://futureenergysp.com/index.php/tre/article/view/30/35

[26] A. G. Lazaropoulos, "Main Line Fault Localization Methodology in Smart Grid– Part 1: Extended TM2 Method for the Overhead Medium-Voltage Broadband over Power Lines Networks Case," *Trends in Renewable Energy*, vol. 3, no. 3, pp. 2-25, Dec. 2017. [Online]. Available: http://futureenergysp.com/index.php/tre/article/view/36

[27] A. G. Lazaropoulos, "Main Line Fault Localization Methodology in Smart Grid– Part 2: Extended TM2 Method, Measurement Differences and L1 Piecewise Monotonic Data Approximation for the Overhead Medium-Voltage Broadband over Power Lines Networks Case," *Trends in Renewable Energy*, vol. 3, no. 3, pp. 26-61, Dec. 2017. [Online]. Available: http://futureenergysp.com/index.php/tre/article/view/37

[28] A. G. Lazaropoulos, "Main Line Fault Localization Methodology in Smart Grid– Part 3: Main Line Fault Localization Methodology (MLFLM)," *Trends in Renewable Energy*, vol. 3, no. 3, pp. 62-81, Dec. 2017. [Online]. Available: http://futureenergysp.com/index.php/tre/article/view/38

[29] A. G. Lazaropoulos, "Special Cases during the Detection of the Hook Style Energy Theft in Overhead Low-Voltage Power Grids through HS-DET Method – Part 1: High Measurement Differences, Very Long Hook Technique and "Smart" Hooks," *Trends in Renewable Energy*, vol. 5, no. 1, pp. 60-89, Jan. 2019. [Online]. Available: http://futureenergysp.com/index.php/tre/article/view/82/pdf

[30] A. G. Lazaropoulos, "Special Cases during the Detection of the Hook Style Energy Theft in Overhead Low-Voltage Power Grids through HS-DET Method – Part 2: Different Measurement Differences, Feint "Smart" Hooks and Hook Interconnection Issues," *Trends in Renewable Energy*, vol. 5, no. 1, pp. 90-116, Jan. 2019. [Online]. Available: http://futureenergysp.com/index.php/tre/article/view/83/pdf

[31] A. G. Lazaropoulos, "The Role of Information Technology Department against the Hook Style Energy Theft in Smart Cities – Ad-Hoc Overhead Low-Voltage Broadband over Power Lines (OV LV BPL) Networks," *Trends in Renewable Energy*, vol. 5, no. 2, pp. 117-150, Apr. 2019. [Online]. Available: http://futureenergysp.com/index.php/tre/article/download/93/pdf